A coherently stimulated Brillouin spectrometer

Joel N. Johnson[1,2*], Peter T. Rakich[3], Co Authors[4], Ryan O. Behunin[1,2*]

[1]Department of Applied Physics and Materials Science, Northern Arizona University, Flagstaff, 86011, AZ, USA.
[2]Center for Materials Interfaces in Research and Applications, Flagstaff, 86011, AZ, USA.
[3]Department of Applied Physics, Yale University, New Haven, 06520, CT, USA.
[4]Department, Organization, Street, City, 610101, State, Country.

*Corresponding author(s). E-mail(s): joel.johnson@nau.edu; ryan.behunin@nau.edu;

Abstract

Lorem ipsum dolor sit amet, consectetur adipiscing elit. Sed non risus. Suspendisse lectus tortor, dignissim sit amet, adipiscing nec, ultricies sed, dolor. Cras elementum ultrices diam. Maecenas ligula massa, varius a, semper congue, euismod non, mi. Proin porttitor, orci nec nonummy molestie, enim est eleifend mi, non fermentum diam nisl sit amet erat. Duis semper. Duis arcu massa, scelerisque vitae, consequat in, pretium a, enim. Pellentesque congue. Ut in risus volutpat libero pharetra tempor. Cras vestibulum bibendum augue. Praesent egestas leo in pede. Praesent blandit odio eu enim. Pellentesque sed dui ut augue blandit sodales. Vestibulum ante ipsum primis in faucibus orci luctus et ultrices posuere cubilia Curae; Aliquam nibh. Mauris ac mauris sed pede pellentesque fermentum. Maecenas adipiscing ante non diam sodales hendrerit.

Keywords: Brillouin scattering, phonon spectrometer, photonics, femtowatt, pump-probe, instrument, room-temperture, nano-acousto-optic devices

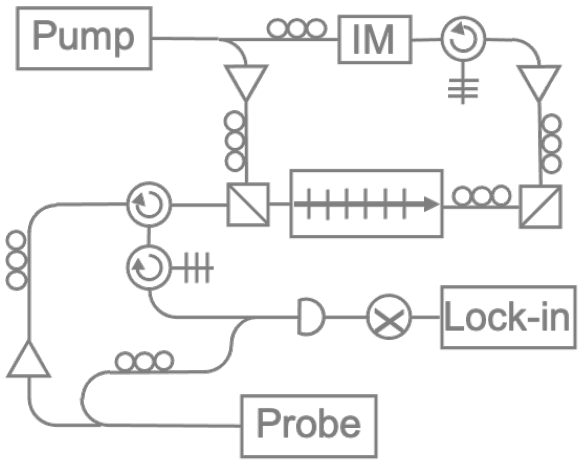

Fig. 1 CABS design diagram

Brillouin scattering is the inelastic scattering of light from acoustic phonons. Spontaneous Brillouin scattering is the scattering of light specifically with thermodynamic fluctuations in a material. Sufficient optical power elevates this spontaneous process into stimulated Brillouin scattering: a regime in which the optical fields augment the optical properties of the material, greatly enhancing the optomechanical response. This occurs as the backscattered (e.g. Stokes) light beats with the incident pump light to induce an electrostrictive modulation that reinforces the acoustic phonons in the material. It would be desirable to introduce a high-powered fourth optical field dedicated to electrostrictive reinforcement, further stimulating the acoustic field, however phase matching conditions require that its frequency and wavevector be identical to that of the backscattered light, preventing distinguishability.

In this work, we present a coherently stimulated Brillouin spectrometer that utilizes a detuned pump-probe design to perform traveling-wave phonon spectroscopy at scales previously unachievable with traditional stimulated Brillouin techniques. With this method, we achieve sub-10 femtowatt sensitivity and enable traveling-wave phonon spectroscopy at the micrometer scale. We demonstrate the capabilities of the instrument by observing Brillouin scattering at room temperature in 1 centimeter of UHNA3 fiber and 100 micrometers of bulk carbon disulfide liquid. This instrument opens the door to nanometer-scale Brillouin spectroscopy with usage of higher optical powers and enables the characterization and development of novel nano-acousto-optic devices.

Results

Instrument Design

In Fig. 1, a pump and Stokes signal is synthesized from a single tunable laser source for coherent stimulation of the sample. The pump signal (ω_{Pump}) is amplified by an erbium-doped fiber amplifier (EDFA) and passed through a variable optical attenuator (VOA). The output is then polarization-controlled to reflect at a polarizing beam splitter (PBS) for injection into the sample. For Stokes synthesis, an AC signal (Ω) is supplied to an intensity modulator with carrier frequency nulled and a tunable filter is used to select one side band output ($\omega_{Pump} - \Omega$). This Stokes signal is then amplified by an EDFA, passed through a VOA, and polarization-controlled to reflect at a second PBS for couter-propagating injection into the sample.

A separate tunable laser ($\omega_{Probe} = \omega_{Pump} + \Delta k$) is used to synthesize the probe and local oscillator (LO). Probe light is amplified by an EDFA and fed through a VOA. A polarization controller aligns the polarization axis of the probe light for transmission through the first PBS and copropagation with the pump into the sample. Backscattered probe light retraces through the first PBS while the orthogonally polarized Stokes light is diverted along a different path. The backscattered signal ($\omega_{Signal} = \omega_{Probe} + \Omega$) then routes through two subsequent circulators for spectral filtering by a 5 GHz bandpass tunable filter which passes the frequency-shifted probe light while rejecting any reflected probe light as well as any reflected, transmitted, or backscattered light from the pump and Stokes that was not diverted by the PBS. The filtered signal combines via a 99-1 splitter with the frequency upshifted LO ($\omega_{Probe} + 40MHz$) which has been polarization-controlled to be in parallel with the signal polarization. This heterodyned signal ($\Omega + 40MHz$) is then captured by a photodiode detector, heterodyned again with an AC signal ($\Omega - 5MHz$) by a radio frequency (RF) mixer, and read into a lock-in amplifier for data collection. Both AC signals, for the RF mixer and Stokes synthesis, are swept together when taking a measurement so as to maintain a constant 45 MHz lock-in frequency.

Measurements

We consider two example targets to demonstrate the capabilities of the instrument, one fiber-coupled and one bulk material. Fig. 2 shows the spectra captured for 1 cm of UHNA3 fiber. The spectral shape is that of the expected lorentzian function, with the peak ([9.18 GHz]) indicating the Brillouin resonance frequency and the FWHM ([80 MHz]) indicating the dissipation rate of the fiber. [comparison to regular SBS for some measurable length of UHNA3?]

Fig. shows the spectral measurements achieved by the instrument, overlaid with finite-difference simulation data. In Fig. we see the expected lorentzian spectral shape in good alignment with simulation data for guided longitudinal modes in the core of the UHNA3 fiber. In Fig. , however, we see a distortion of this lorentzian shape. This is expected for partially unguided longitudinal modes, such as is the case for a bulk liquid filling the volume of a ...

Fig. 2 shows a measurement of 1cm of UHNA3 fiber.

First, we measured Brillouin scattering in a 1-centimeter-long UHNA3 fiber at room temperature and with sub-Watt optical power (Fig.). Figure , clearly displays the Brillouin scattering features with remarkable signal-to-noise ratio, highlighting the effectiveness of

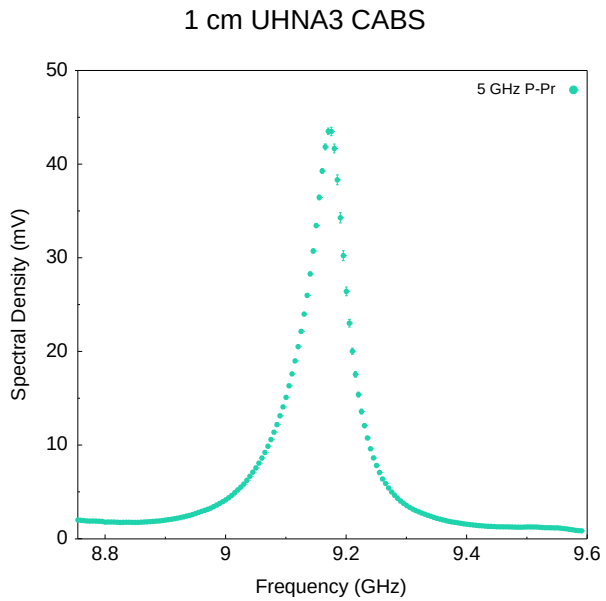

Fig. 2 1cm UHNA3 [needs fit]

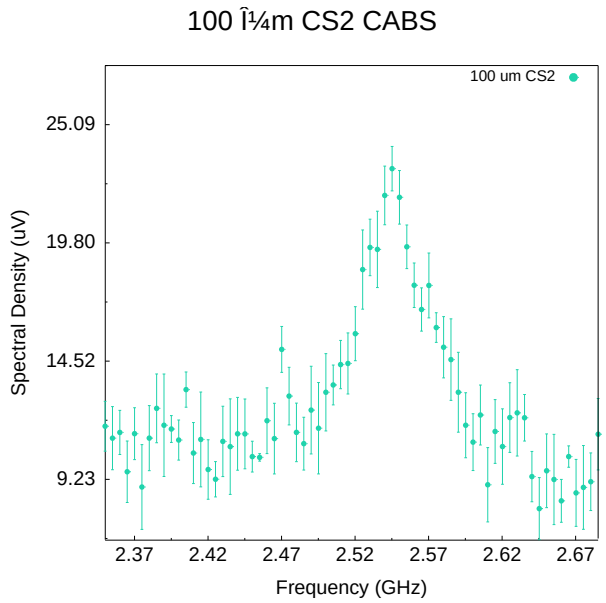

Fig. 3 100um CS2

our apparatus in isolating the backscattered probe light. This observation serves as one of the main showcases of the instrument's capability.

Next, we performed Brillouin scattering measurements on a 4-millimeter-thick bulk carbon disulfide sample in a free-space optics arrangement. The observed spectrum, presented in Figure 2, exhibits well-resolved Brillouin scattering peaks. This successful measurement in a bulk sample demonstrates the versatility and adaptability of our instrument to various experimental configurations, further emphasizing the instrument's capability.

Lastly, we conducted a measurement in a 1-millimeter-long UHNA3 fiber under low-power conditions, with only 10 microwatts of power at the sample. Despite the reduced sample length and low power, the instrument's sensitivity allowed us to observe distinct

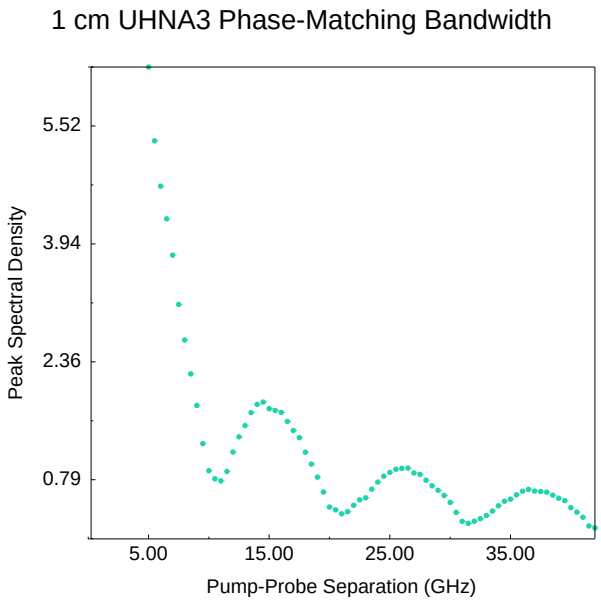

Fig. 4 Phase-matching sinc func

Brillouin scattering features in the spectrum, as illustrated in Figure 3. This result underscores the potential of our spectrometer for nanoscale measurements and serves as a demonstration of the instrument's sensitivity, defining the sensitivity floor of the apparatus.

These three observations collectively showcase the high sensitivity, broad applicability, and impressive capabilities of our coherent stimulated phonon spectrometer in measuring Brillouin scattering across different sample types, scales, and power levels.

Discussion

Lorem ipsum dolor sit amet, consectetuer adipiscing elit. Ut purus elit, vestibulum ut, placerat ac, adipiscing vitae, felis. Curabitur dictum gravida mauris. Nam arcu libero, nonummy eget, consectetuer id, vulputate a, magna. Donec vehicula augue eu neque. Pellentesque habitant morbi tristique senectus et netus et malesuada fames ac turpis egestas. Mauris ut leo. Cras viverra metus rhoncus sem. Nulla et lectus vestibulum urna fringilla ultrices. Phasellus eu tellus sit amet tortor gravida placerat. Integer sapien est, iaculis in, pretium quis, viverra ac, nunc. Praesent eget sem vel leo ultrices bibendum. Aenean faucibus. Morbi dolor nulla, malesuada eu, pulvinar at, mollis ac, nulla. Curabitur auctor semper nulla. Donec varius orci eget risus. Duis nibh mi, congue eu, accumsan eleifend, sagittis quis, diam. Duis eget orci sit amet orci dignissim rutrum.

Nam dui ligula, fringilla a, euismod sodales, sollicitudin vel, wisi. Morbi auctor lorem non justo. Nam lacus libero, pretium at, lobortis vitae, ultricies et, tellus. Donec aliquet, tortor sed accumsan bibendum, erat ligula aliquet magna, vitae ornare odio metus a mi. Morbi ac orci et nisl hendrerit mollis. Suspendisse ut massa. Cras nec ante. Pellentesque a nulla. Cum sociis natoque penatibus et magnis dis parturient montes, nascetur ridiculus mus. Aliquam tincidunt urna. Nulla ullamcorper vestibulum turpis. Pellentesque cursus luctus mauris.

Methods

Figures were made using Go and the gonum/plot library.

References

Supplementary Information:
A Coherently Stimulated Brillouin Spectrometer

Contents

Appendix A Phase Matching

A.1 Relaxation of Phase Matching Conditions

A.2 Phase Matching Bandwidth Experiments

A.3 Theoretical Comparison of Phase Matching Bandwidth

Appendix B Coupled-Wave Equations

Here we derive the coupled wave equations that describe coherent stimulated Brillouin scattering involving a pump, Stokes, probe, and backscattered optical field given respectively by

$$\tilde{E}_P(z,t) = A_P e^{i(k_P z - \omega_P t)} + c.c. \tag{B1}$$

$$\tilde{E}_S(z,t) = A_S e^{i(k_S z - \omega_S t)} + c.c. \tag{B2}$$

$$\tilde{E}_{Pr}(z,t) = A_{Pr} e^{i(k_{Pr} z - \omega_{Pr} t)} + c.c. \tag{B3}$$

$$\tilde{E}_{Sig}(z,t) = A_{Sig} e^{i(k_{Sig} z - \omega_{Sig} t)} + c.c. \tag{B4}$$

and a common acoustic field given by

$$\tilde{\rho}(z,t) = \rho_0 + \rho(z,t) e^{i(qz - \Omega t)} + c.c., \tag{B5}$$

where $\Omega = \omega_P - \omega_S$ and $q = k_P - k_S = 2k_P$.

B.1 Acoustic Field

We start by assuming that the material obeys the acoustic wave equation,

$$\frac{\partial^2 \tilde{\rho}}{\partial t^2} - \Gamma' \nabla^2 \frac{\partial \tilde{\rho}}{\partial t} - v^2 \nabla^2 \tilde{\rho} = \nabla \cdot \vec{f}, \tag{B6}$$

where v is the sound speed in the material and Γ' is a damping parameter given by

$$\Gamma' = \frac{1}{\rho}\left[\frac{4}{3}\eta_s + \eta_b + \frac{\kappa}{C_p}(\gamma - 1)\right], \tag{B7}$$

where η_s and η_b are the shear and bulk viscosity coefficients of the material, respectively. The source term on the right side of Eq. (B6) is the divergence of the electrostrictive force:

$$\vec{f} = \nabla p_{st} = \nabla \cdot \left[-\frac{1}{2}\epsilon_0 \gamma_e \Big(\langle \tilde{E}_P \cdot \tilde{E}_S \rangle + \langle \tilde{E}_{Pr} \cdot \tilde{E}_{Sig} \rangle \Big) \right], \tag{B8}$$

which yields, after applying the slowly varying amplitude approximation,

$$\nabla \cdot \vec{f} = \epsilon_0 \gamma_e q^2 (A_P A_S^* + A_{Pr} A_{Sig}^* e^{i\Delta k z}), \tag{B9}$$

Where $\Delta k = (k_{Pr} - k_{Sig}) - (k_P - k_S)$ is the phase mismatch between the four optical fields. Only two electrostrictive terms survive terms after accounting for the orthogonal polarization of the pump and Stokes fields with respect to that of the probe and backscattered signal. Inserting this electrostrictive force term and the acoustic field (Eq. (B5)) into Eq. (B6) and assuming a slowly varying acoustic amplitude we find

$$-2i\Omega \frac{\partial \rho}{\partial t} - \Gamma' 2iq^2 \Omega \rho - 2iqv^2 \frac{\partial \rho}{\partial z} = \epsilon_0 \gamma_e q^2 (A_P A_S^* + A_{Pr} A_{Sig}^* e^{i\Delta k z}), \tag{B10}$$

which can be restated in terms of the Brillouin linewidth, $\Gamma_B = q^2\Gamma'$, as

$$-2i\Omega\frac{\partial\rho}{\partial t} - 2i\Omega\Gamma_B\rho - 2iqv^2\frac{\partial\rho}{\partial z} = \epsilon_0\gamma_e q^2(A_P A_S^* + A_{Pr}A_{Sig}^* e^{i\Delta kz}). \tag{B11}$$

Given the phonon dispersion relations $\Omega_B = |q_B|v$ and $\Omega^2 = q^2\left(v^2 - i\Omega\Gamma'\right)$, Eq. (B11) can be rewritten as

$$-2i\Omega\frac{\partial\rho}{\partial t} + \left(\Omega^2 - \Omega^2 - i\Omega\Gamma_B\right)\rho - 2iqv^2\frac{\partial\rho}{\partial z} = \epsilon_0\gamma_e q^2(A_P A_S^* + A_{Pr}A_{Sig}^* e^{i\Delta kz}). \tag{B12}$$

We take the common assumption that the phonon propagation distance is small compared to the distance over which the source term varies significantly, which allows the spatial derivative term in Eq. (B12). We further assume steady-state conditions such that the time derivative term also vanishes, leaving

$$(\Omega_B^2 - \Omega^2 - i\Omega\Gamma_B)_\rho = \epsilon_0\gamma_e q^2(A_P A_S^* + A_{Pr}A_{Sig}^* e^{i\Delta kz}). \tag{B13}$$

We thus find the acoustic field amplitude to be

$$\rho(z,t) = \epsilon_0\gamma_e q^2\frac{A_P A_S^* + A_{Pr}A_{Sig}^* e^{i\Delta kz}}{\Omega_B^2 - \Omega^2 - i\Omega\Gamma_B}. \tag{B14}$$

B.2 Optical Fields

We now turn to the spatial evolution of the optical fields, described by the wave equation,

$$\frac{\partial^2\tilde{E}_i}{\partial z^2} - \frac{n^2}{c^2}\frac{\partial^2\tilde{E}_i}{\partial t^2} = \frac{1}{\epsilon_0 c^2}\frac{\partial^2\tilde{P}_i}{\partial t^2}, \tag{B15}$$

where i denotes the four optical fields, namely: pump, Stokes, probe, and backscattered signal. The total nonlinear polarization that gives rise to the source term in the wave equation is given by

$$\tilde{P} = \epsilon_0\Delta\chi\tilde{E} = \epsilon_0\Delta\epsilon\tilde{E} = \epsilon_0\rho^{-1}\gamma_e\tilde{\rho}\tilde{E}. \tag{B16}$$

The parts of $\tilde{P}$ that can act as phase-matched source terms for the optical fields are

$$\tilde{P}_P = p_P e^{i(k_P z - \omega_P t)} + c.c. = \frac{1}{2}\epsilon_0\rho_0^{-1}\gamma_e\rho A_S e^{i(k_P z - \omega_P t)} \tag{B17}$$

$$\tilde{P}_S = p_S e^{i(-k_S z - \omega_S t)} + c.c. = \frac{1}{2}\epsilon_0\rho_0^{-1}\gamma_e\rho^* A_P e^{i(-k_S z - \omega_S t)} \tag{B18}$$

$$\tilde{P}_{Pr} = p_{Pr} e^{i(k_{Pr} z - \omega_{Pr} t)} + c.c. = \frac{1}{2}\epsilon_0\rho_0^{-1}\gamma_e\rho A_{Sig} e^{i(k_{Pr} z - \omega_{Pr} t)} e^{i\Delta kz} \tag{B19}$$

$$\tilde{P}_{Sig} = p_{Sig} e^{i(-k_{Sig} z - \omega_{Sig} t)} + c.c. = \frac{1}{2}\epsilon_0\rho_0^{-1}\gamma_e\rho^* A_{Pr} e^{i(-k_{Sig} z - \omega_{Sig} t)} e^{-i\Delta kz}. \tag{B20}$$

Inserting the optical fields (Eqs. B1-B4) and phase-matched source terms (Eqs. B17-B20) into Eq. (B15), we obtain

$$\frac{\partial A_P}{\partial z} + \frac{n}{c}\frac{\partial A_P}{\partial t} = \frac{i\omega_P\gamma_e}{2nc\rho_0}\rho A_2 \tag{B21}$$

$$-\frac{\partial A_S}{\partial z} + \frac{n}{c}\frac{\partial A_S}{\partial t} = \frac{i\omega_S\gamma_e}{2nc\rho_0}\rho^* A_P \tag{B22}$$

$$\frac{\partial A_{Pr}}{\partial z} + \frac{n}{c}\frac{\partial A_{Pr}}{\partial t} = \frac{i\omega_{Pr}\gamma_e}{2nc\rho_0}\rho A_{Sig} \tag{B23}$$

$$-\frac{\partial A_{Sig}}{\partial z} + \frac{n}{c}\frac{\partial A_{Sig}}{\partial t} = \frac{i\omega_{Sig}\gamma_e}{2nc\rho_0}\rho^* A_{Pr} \tag{B24}$$

We again assume steady-state conditions, allowing the time derivative term to be dropped. Plugging in the acoustic field amplitude (Eq. B14), we arrive at the coupled-amplitude wave equations for the optical fields,

$$\frac{\partial A_P}{\partial z} = \frac{i\epsilon_0 \omega_P q^2 \gamma_e^2}{2nc\rho_0} \frac{A_P|A_S|^2 + A_{Pr}A_{Sig}^* A_S e^{i\Delta kz}}{\Omega_B^2 - \Omega^2 - i\Omega\Gamma_B} \tag{B25}$$

$$\frac{\partial A_S}{\partial z} = -\frac{i\epsilon_0 \omega_S q^2 \gamma_e^2}{2nc\rho_0} \frac{|A_P|^2 A_S^* + A_{Pr}A_{Sig}^* A_P e^{i\Delta kz}}{\Omega_B^2 - \Omega^2 - i\Omega\Gamma_B} \tag{B26}$$

$$\frac{\partial A_{Pr}}{\partial z} = \frac{i\epsilon_0 \omega_{Pr} q^2 \gamma_e^2}{2nc\rho_0} \frac{A_P A_S^* A_{Sig} + A_{Pr}|A_{Sig}|^2 e^{i\Delta kz}}{\Omega_B^2 - \Omega^2 - i\Omega\Gamma_B} \tag{B27}$$

$$\frac{\partial A_{Sig}}{\partial z} = -\frac{i\epsilon_0 \omega_S q^2 \gamma_e^2}{2nc\rho_0} \frac{A_P A_S^* A_{Pr} + |A_{Pr}|^2 A_{Sig}^* e^{i\Delta kz}}{\Omega_B^2 - \Omega^2 - i\Omega\Gamma_B} \tag{B28}$$

Integrating Eq. B28 along the effective length gives the amplitudes of each optical field,

$$A_P = \frac{i\epsilon_0 \omega q^2 \gamma_e^2}{2nc\rho_0} \frac{A_P|A_S|^2 + A_{Pr}A_{Sig}^* A_S}{\Omega_B^2 - \Omega^2 - i\Omega\Gamma_B} \frac{e^{-i\Delta kL} - 1}{\Delta k}, \tag{B29}$$

$$A_S = -\frac{i\epsilon_0 \omega q^2 \gamma_e^2}{2nc\rho_0} \frac{|A_P|^2 A_S^* + A_{Pr}A_{Sig}^* A_P}{\Omega_B^2 - \Omega^2 - i\Omega\Gamma_B} \frac{e^{-i\Delta kL} - 1}{\Delta k}, \tag{B30}$$

$$A_{Pr} = -\frac{i\epsilon_0 \omega q^2 \gamma_e^2}{2nc\rho_0} \frac{A_P A_S^* A_{Sig} + A_{Pr}|A_{Sig}|^2}{\Omega_B^2 - \Omega^2 - i\Omega\Gamma_B} \frac{e^{-i\Delta kL} - 1}{\Delta k}, \tag{B31}$$

$$A_{Sig} = -\frac{i\epsilon_0 \omega q^2 \gamma_e^2}{2nc\rho_0} \frac{A_P A_S^* A_{Pr} + |A_{Pr}|^2 A_{Sig}^*}{\Omega_B^2 - \Omega^2 - i\Omega\Gamma_B} \frac{e^{-i\Delta kL} - 1}{\Delta k}. \tag{B32}$$

The intensity of the backscattered signal is then given by the square of the magnitude of its amplitude,

$$I_{Sig} = \frac{\epsilon_0^2 \omega^2 q^4 \gamma_e^4}{4n^2 c^2 \rho_0^2} \frac{I_P I_S I_{Pr}}{(\Omega_B - \Omega)^4 - \Omega^2 \Gamma_B^2} L^2 sinc^2\left(\frac{\Delta kL}{2}\right) \tag{B33}$$

Here we have taken the real part and dropped the very small terms containing the signal amplitude. Defining the intensities as $I_i = 2n\epsilon_0 c A_i A_i^*$, the backscattered signal intensity is reduced to [see green writing to far right in onenote coupled wave equations of CABS]

To find the power of the backscattered signal, we would integrate this intensity over the effective area. Approximated for fiber as πr^2 where r is the effective mode field diameter, this becomes

$$P_{Sig} = \pi r^2 \frac{\epsilon_0^2 \omega^2 q^4 \gamma_e^4}{4n^2 c^2 \rho_0^2} \frac{P_P P_S P_{Pr}}{(\Omega_B - \Omega)^4 - \Omega^2 \Gamma_B^2} L^2 sinc^2\left(\frac{\Delta kL}{2}\right). \tag{B34}$$